RSC Advances

ROYAL SOCIETY OF CHEMISTRY

www.rsc.org/advances

Freestanding and flexible Graphene wrapped MnO_2/MoO_3 nanoparticles based asymmetric supercapacitors for high energy density and output voltage

Congxing Yang,[a] Yuling Shi,[a] Nishuang Liu,*[a] Jiayou Tao,[a] Siliang Wang,[a] Weijie Liu,[a] Yumei Wang,[a] Jun Su,[a] Luying Li[a], Changping Yang[b] and Yihua Gao*[ab]

Asymmetric supercapacitors (ASC) based on freestanding membranes with high energy density and high output voltage by simply pre-reduced and vacuum filtering method are reported. Reduced graphene oxide (rGO) coated MnO_2 nanospheres and rGO coated MoO_3 nanoparticles composites are selected as the positive and the negative materials of the devices, respectively. The ASC has a high operation voltage window of 2.0 V in a hydrogen electrolyte, a high energy density of 34.6 mWh cm^{-3} at a power density of 100 mW cm^{-3}, and a high volumetric capacitance of 62.7 F cm^{-3} at a current density of 0.1 A cm^{-3}. Especially, the ASC exhibits excellent cycling performance of 94.2% capacitance retention after over 3000 cycles. This strategy of designing the hybridized structure for freestanding and flexible ASC provides a promising route for next-generation supercapacitors with high energy density and high output voltage.

Introduction

Bendable freestanding films emerge to garner major interest recently because they have various potential applications in energy storage, catalysis, environment and sensing.[1-3] Particularly, flexible energy storage devices such as supercapacitors(SC) and batteries, which extensively rely on such bendable film electrodes, are receiving more and more attention with the increasing demand for wearable and portable consumer electronics.[4, 5] However, these SC suffer from a lower energy density, which obstacle to their potential applications.[6, 7] According to the equation $E = 0.5\ CU^2$, the increase of energy (E) can be achieved by maximizing the specific capacitance (C) and the operation voltage (U).[8] Organic and solid electrolyte based ASC can effectively increase the operation voltage to realize energy density boost. However, their low capacitance and unfriendly electrolyte undermine their overall effectiveness for ASC.

MnO_2 and MoO_3 are both the most thoroughly investigated for supercapacitor applications because of their remarkable theoretical specific capacitance, natural abundance, low cost and environmental friendliness.[9-12] Fortunately, due to the big work function difference (4.4 eV of MnO_2 and 6.9 eV of MoO_3, respectively), it is easy to acquire widest potential window while choose MnO_2 as a positive electrode material and MoO_3 as a negative electrode material.[13-16] However, the poor electrical conductivity seriously hinders to achieve the theoretical specific capacitance in the experiment. Graphene, as a two dimensional carbon material, has drawn considerable attention as an electrode material for supercapacitor because of its unique properties such as high electrical conductivity, flexibility, mechanical strength, superior chemical stability and broad electrochemical window.[17] Unfortunately, freestanding films composed of graphene nanostructure are readily to be restacked into "graphite" due to the tremendous Van der Waals attraction during the fabrication process, which leads to poor penetration of electrolyte into the graphene nanosheets and a small active surface area.[18] Some reporters want to escape this problem by making a gel.[19, 20] However, it is obvious that it is unacceptable for flexible and freestanding film with high volumetric energy density.[21] The method of making sandwich structure from graphene and pseudocapacitance materials is valid to alleviate the problem, regrettably, those works with high energy

[a]Center for Nanoscale Characterization & Devices (CNCD), Wuhan National Laboratory for Optoelectronics (WNLO), School of Physics, Huazhong University of Science and Technology (HUST), LuoyuRoad 1037, Wuhan 430074, P. R. China. E-mail: gaoyihua@hust.edu.cn; nishuang_liu@foxmail.com
[b]Hubei Collaborative Innovation Center for Advanced Organic Chemical Materials. 368 Youvi Avenue. Wuhan 430062. P. R. China

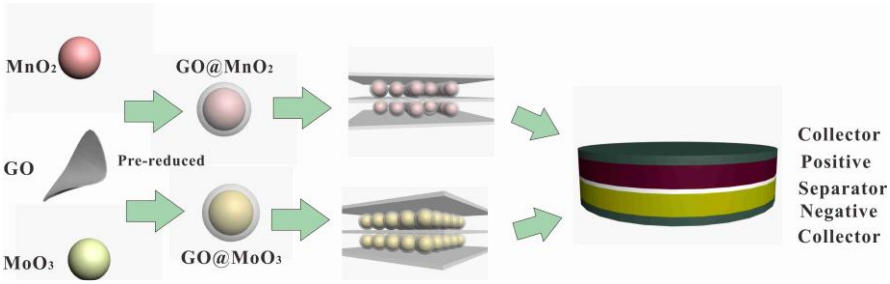

Fig.1 Fabrication process of ASC devices based on Graphene@MnO_2 as positive and Graphene@MoO_3 as negative electrodes in 1M LiCl electrolyte.

density are rarely reported.[22-24]

Herein, we fabricated a flexible ASC based on rGO coated MnO_2 nanoparticles (MnO_2@rGO) for the positive electrode and rGO wrapped nanostructure MoO_3 nanoparticles (MoO_3@rGO) for the negative electrode by simply pre-reduced and vacuum filtering method. The unique nanostructure of graphene is to maintain the flexibility and electronic transmission path of the electrode material.[25] The clearance of different graphene sheets were used to be ion diffusion channel. In addition, MnO_2 and MoO_3 nanoparticles are wrapped by rGO not only to prevent rGO to reunite but also to improve the contact between nanoparticles and rGO. Thus we will benefit for the reaction of Faradic pseudocapacitance, electronic transaction and cyclic stability. Since freestanding graphene-based films have shown more applications compared to individual graphene sheets,[26, 27] and such unique nanostructure to composite freestanding films into ASC has not reported, the freestanding rGO-wrapped nanostructure film (MnO_2@rGO/MoO_3@rGO) ASCs were fabricated. The positive electrode MnO_2@rGO shows a high volume capacitance 343 F cm^{-3}, and the negative electrode shows volume capacitance 200 F cm^{-3}. Importantly, the ASC acquire a high volumetric capacitance of 62.7 F cm^{-3} at a current density of 0.1 A cm^{-3}, excellent cycling performance of 94.2% capacitance retention after over 3000 cycles, and a high energy density of 34.6 mWh cm^{-3} at a power density of 100 mW cm^{-3}. Compared to others researchers on freestanding graphene matrix composite nanostructure ASC, our ASC is flexible and significantly improves both energy density and power density.

Experimental

Materials

GO was prepared by oxidation of natural graphite powder by using a modified Hummers' method. It is easy to prepare the MnO_2 nanoparticles by modified hydrothermal reduction method. By a simply pre-reduced and vacuum filtration procedure, the flexible and freestanding positive electrode material is acquired. The same procedure to fabrication freestanding Graphene@MoO_3 films.

The morphologies, structure, and chemical composition of the samples were characterized by high-resolution field emission SEM (FEI Nova Nano-SEM 450), TEM (FEI Titan G2 60-300), and XRD (PANalytical B.V. X'Pert PRO).

Electrochemical measurements

All the electrochemical measurements were carried out in a two-electrode system at room temperature using Autolab PGSTAT302N (Metrohm AG). The electrochemical impedance spectroscopy was carried out at 10 mHz to 100 kHz with a potential amplitude of 10 mV. The electrochemical tests of the individual electrode were performed in a three electrode cell, in which carbon electrode and Ag/AgCl electrode was used as the counter and reference electrode, respectively. The electrochemical measurements of the ASC were carried out in a two electrode cell at room temperature in 1 M LiCl electrolyte. All of the above electrochemical measurements were carried out by a biologicMP3 electrochemical workstation.

Result and discussion

Characterizations of positive electrode materials

The preparation process for ASC based on rGO is illustrated in Fig. 1. Freestanding membranes are prepared by a simple vacuum filtration and

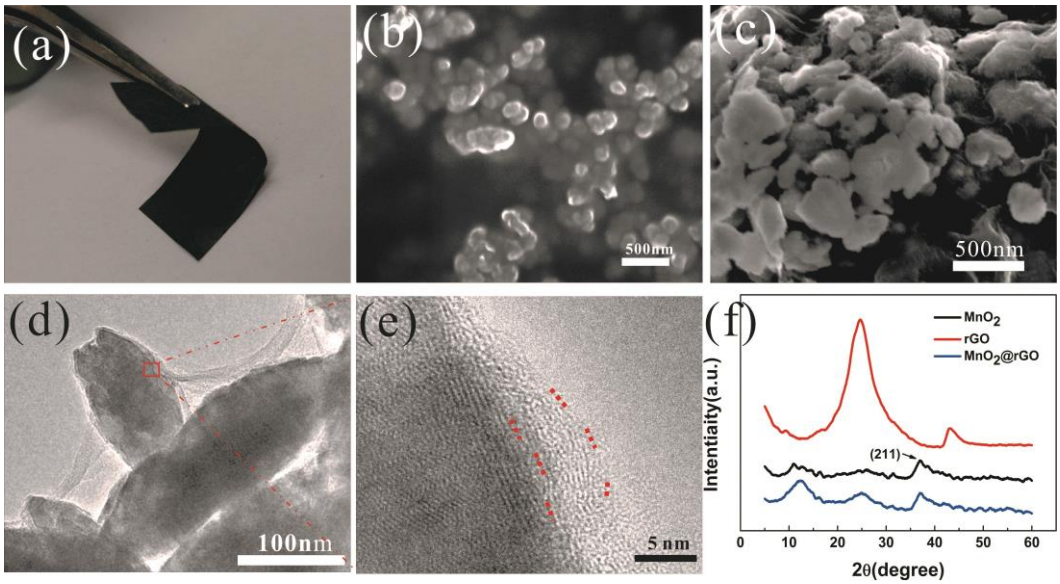

Fig.2 (a) Optical image of MnO_2@rGO film with expected flexibility, (b) TEM image of pure MnO_2 morphology, (c) SEM image of the stacking MnO_2 particles wrapped by rGO, (d, e) Low and high magnification TEM images of MnO_2@rGO composite, (f) XRD patterns of pure MnO_2, pure rGO and MnO2@rGO.

pre-reduced technique. When the films were dried and been annealed, finally assembled the ASC. Particularly, the pre-reduced process before vacuum filtering is necessary, otherwise the freestanding flexible films will become rough and fragile (more details of the experiment are given in ESI†). The morphologies and detailed structures of MoO_3@rGO and MnO_2@rGO composites are characterized by both SEM and TEM observations. Fig. 2a shows the optical image of freestanding MnO_2@rGO compound film with wonderful flexibility. TEM image of pure MnO_2 particles is shown in Fig. 2b. The diameters of the particles are about 100-160 nm. SEM image Fig. 2c shows the freestanding film surface of the MnO_2 nanoparticles which were wrapped by rGO. The average diameters of fusiform MnO_2@rGO particles are around 110–190 nm.

Adjacent graphene films as a framework support freestanding structure. The low and high magnification TEM images of MnO_2 @rGO composites demonstrate the typical crystalline texture of MnO_2 nanoparticles which are tightly enwrapped by graphene sheets (Fig. 2 d and e). The X-ray diffraction (XRD) pattern samples are presented in Fig. 2f. The samples are poorly crystallized and a wide peak at 37.5 °can be clearly observed. This can be ascribed to the (211) diffraction peak of α-MnO_2 (ICDD-JCPDS Card no. 44-0141).

completely，they are cut to a suitable area and then

Cyclic voltammetry (CV) and Galvanostatic charge–discharge(GCD) curses are generally used to characterize the capacitive behavior of an eletrode material. Fig. 3a shows the type CV curves of a freestanding MnO_2@rGO film (the resistance is 30.14 Ω cm^{-2}, the resistivity is $18.84*10^{-3}$ Ω cm^{-1}), approaching the ideal capacitive behavior. This is ascribed to the highly conductive graphene wrapped on the surface of MnO_2 nanoparticles. According to Y. Gogotsi and P. Simon's perspective,[28] the volumetric capacitance (or areal capacitance) of our devices is calculated. The freestanding film exhibits high specific volumetric capacitances of 268 F cm^{-3} and 110 F cm^{-3} at scan rate 5 mV s^{-1} and 100 mV s^{-1} in 1 M LiCl aqueous solution (based on the total volume of the free-standing MnO_2@rGO film), respectively. The specific energy density (E, Wh cm^{-3}) and power density (P, W cm^{-3}) for a supercapacitor cell can be calculated using the following equations: $E = 0.5 CU^2$ and $P = Et^{-1}$, where C is the specific capacitance of SC, U is voltage change, *t* is discharge time. Fig. 3b shows the Ragone plot for the energy density and the power density of the freestanding MnO_2@rGO film, which is calculated from Fig. 3a. The GCD curves of the freestanding MnO_2@rGO film show nearly linear and symmetrical curves (Fig. 3c), thus demonstrate the excellent capacitor performance of the sample.

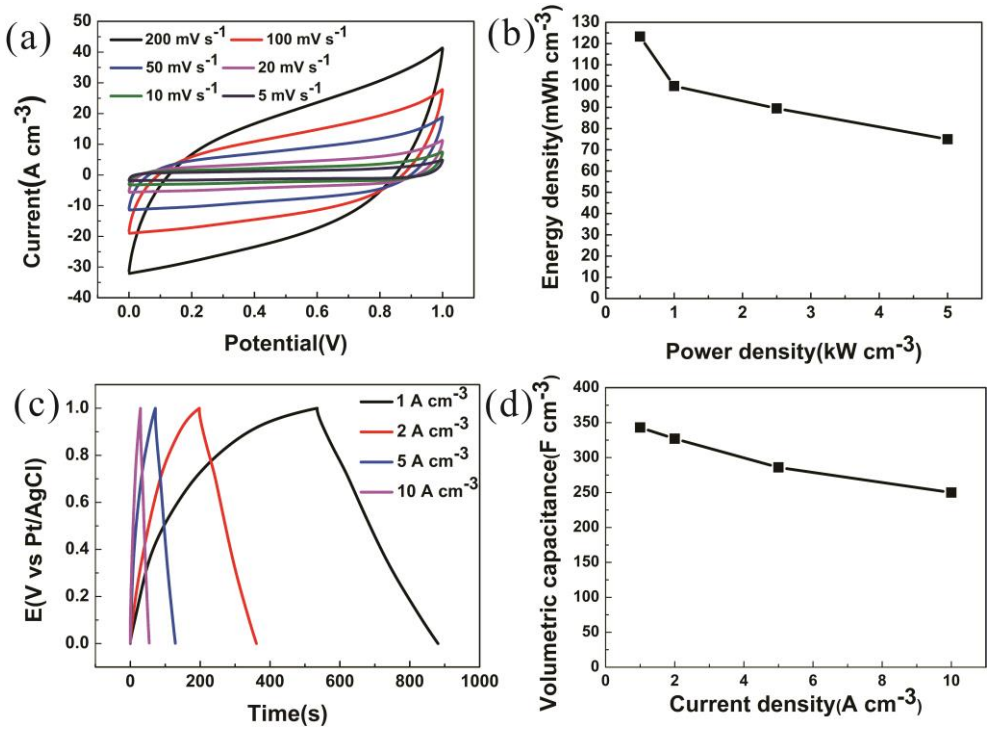

Fig.3 Electrochemical performance of freestanding MnO_2@rGO electrode in a three-electrode configuration: (a) CV cures of composite at different scan rates, (b) Ragone plots of our electrode at different scan rates, (c) GCD curves at various current density, (d) Specific volume capacitance at various current density.

Fig. 3d exhibits the specific capacitances from GCD curves of the freestanding MnO_2@rGO film. The freestanding film exhibits high specific volumetric capacitances of 343 F cm^{-3} and 250 F cm^{-3} at a current density of 1 A g^{-1} and 10 A g^{-1} in 1 M LiCl aqueous solution.

Characterizations of negative electrode materials

In spite of abundant researches on positive electrodes, studies on the negative electrode materials with transition metal oxides have been limited due to the unsatisfactory capacitive performance or high cost of several types of electrode materials.[29,41,42,43] MoO_3 is low cost and layer-structured material, which facilitates the injection of different electrolyte ions into the free spaces, thus creating better electrochemical properties.[30, 31]

The corresponding detailed structures of pure MoO_3 nanoparticles and MoO_3@rGO composites surface were also individually characterized by both SEM and TEM. Fig. 4a shows the optical image of freestanding MoO_3@rGO film with wonderfully flexibility. SEM images Fig. 4b and c demonstrate nanostructure of pure MoO_3 nanoparticles and MoO_3@rGO nanoparticles. It is obvious that MoO_3 nanoparticles were coated by soft graphene. What is more, the low and high magnification TEM images of MoO_3@rGO composites demonstrate that the typical MoO_3 nanoparticles were tightly enwrapped by graphene sheets (Fig. 4 d and e). Fig. 4 f shows the typical XRD patterns of the pure MoO_3 with very sharp diffraction peaks (JCPDS No.05-0508), indicating a highly crystalline orthorhombic structure (α-MoO_3).[32]

The electrochemical tests of the electrode materials were performed in a three-electrode cell using aqueous 1 M LiCl electrolyte. The freestanding film of MoO_3@rGO composite material exhibits excellent capacitive performance with potential window of -0.9 to 0 V in Fig. 5. The CV measurements show excellent negative volumetric capacitance characteristics with various scan rates in Fig. 5a. Fig. 5b exhibits the Ragone plot for freestanding MoO_3@rGO electrode (the resistance is 19.86 Ω cm^{-2}, the resistivity is 19.41*10^{-3} Ω cm^{-1}). To further quantify the capacitance of the as-obtained hybrid film electrode, a series of GCD measurements are carried out at different current densities, and the typical discharge curves are presented in Fig. 5c and 5d. The freestanding MoO_3@rGO film electrode was

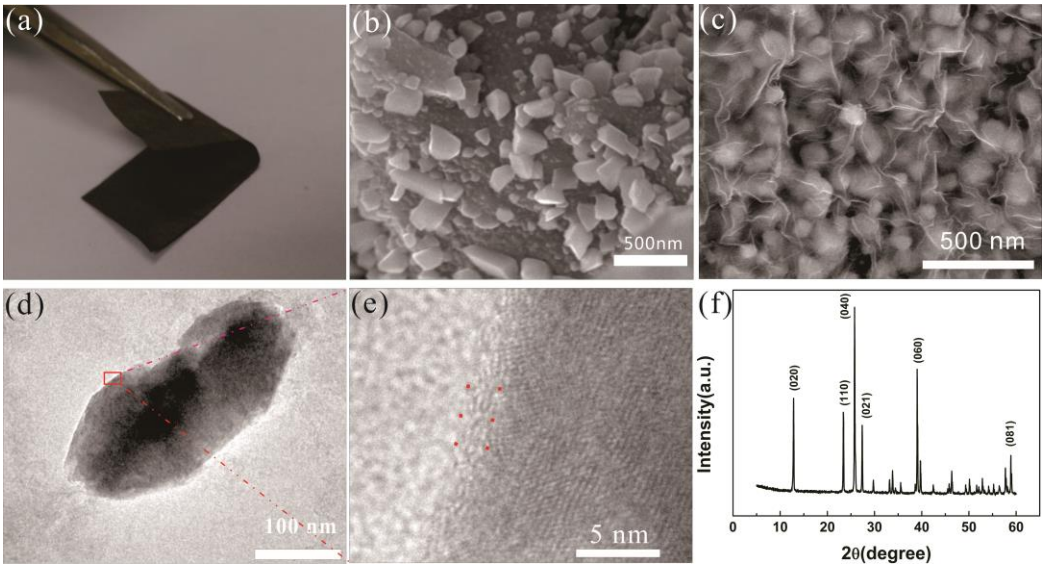

Fig. 4 (a) Optical image of flexible freestanding MoO_3@rGO film; (b) SEM image of pure MoO_3 nanoparticles, (c) SEM image of freestanding MoO_3@rGO composite, (d, e) the detailed structure of the composite using low and high magnification TEM, (f) XRD patterns of pure MoO_3.

able to yield a high volume capacitance of 200 F cm^{-3} at 1 A cm^{-3} based on the total electrode volume. When the current density increased to 10 A cm^{-3}, its capacitance remained at 95 F cm^{-3}.

Hybridized aqueous Asymmetric Supercapacitor

To further investigate the capacitive performance of the flexible freestanding electrodes in a full cell set-up, an ASC is assembled in our study by using a freestanding MnO_2@rGO film as the positive electrode and a freestanding MoO_3@rGO film as the negative electrode in 1M LiCl aqueous electrolyte. Because more negative potential and positive potential can be achieved, both hydrogen and oxygen evolution reactions are supposed to be kinetically limited on these transition metal oxide and graphene composites.[39-40] As a consequence, the operation voltage window can be extended from -0.1 to 1.2 V for MnO_2 nanoparticles and from -1.3 to 0.2 V for MoO_3 nanoparticles in 1M LiCl aqueous electrolyte. In this way, we can still avoid the decomposition of aqueous electrolyte under an operation voltage 2.0 V, reaching a safe performance of both electrodes during long cycling.

In order to verify the high power density and energy density of the ASC, CV measurements and discharge curves are showed in Fig. 6. By expressing the total cell voltage as the sum of the potential range of MnO_2@rGO and MoO_3@rGO electrodes, the hybridized nanostructured ASC can be operated up to 2 V. Fig.6a shows the CV curves of an optimized ASC full cell measured at different scan rates between 0 and 2.0 V in 1 M LiCl electrolyte. These CV curves exhibit distorted rectangular shapes indicating both pseudocapacitance and EDLC contributions. In order to further evaluate the performance of unit cell, we measure discharge curves at various current density (Fig. 6b). Since the ASC two electrodes connect in series, the voltage of ASC to be imposed has no change, the ASC volume capacitor is slightly (base on the total electrode volume) less than 1/4 volume capacitor of each electrode. Fig. 6c show volumetric capacitor of ASC at different current density. The specific capacitance calculated from the GCD curves at a current density of 0.1 A cm^{-3} is 62.7 F cm^{-3}. Profiting from the unique and suitable structure, the ASC exhibits high power density and energy density (Fig. 6d).[33-35] The ASC with a cell voltage of 2.0 V exhibits an energy density of 34.6 mWh cm^{-3}(corresponding energy density 25.2 Wh kg^{-1}) at a power density of 100 mW cm^{-3}(corresponding energy density 72.8 W kg^{-1}). Electrochemical impedance spectroscopy study (EIS) analysis is a principle method to examine the fundamental behavior of electrode materials for supercapacitor. The Nyquist plots reveal the impedance of ASC in the frequency range 100 000–0.01 Hz at an open circuit potential

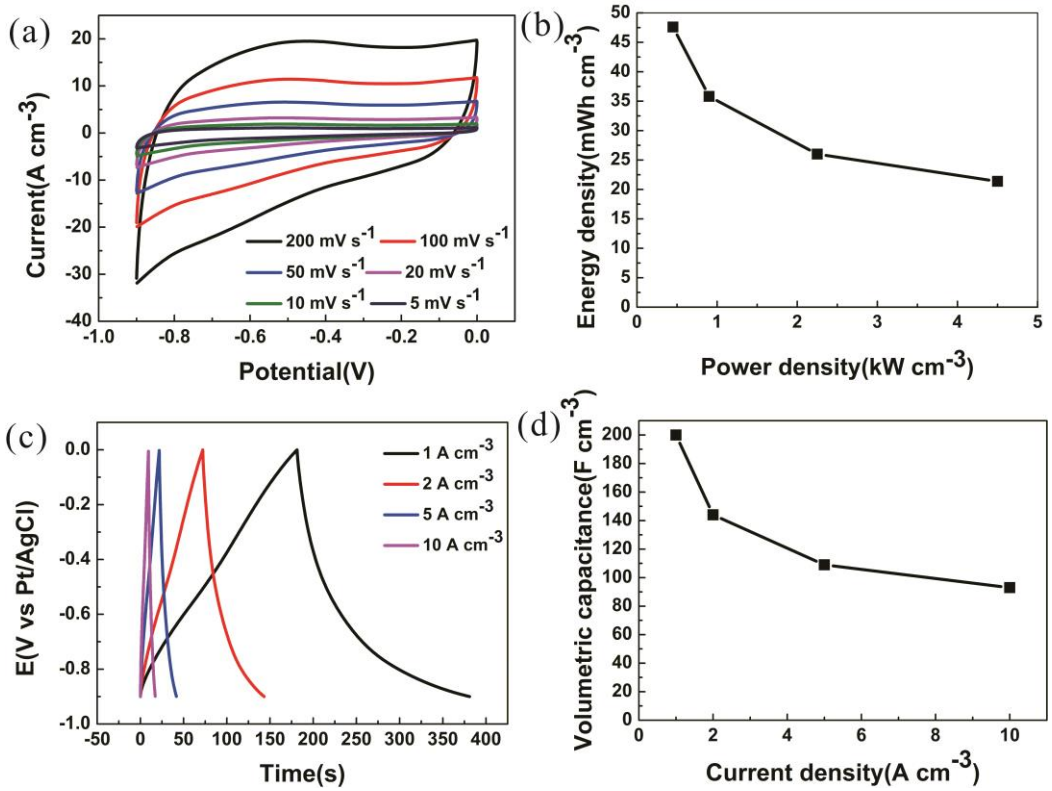

Fig. 5 Electrochemical performance of freestanding MoO_3@rGO electrode in a three-electrode configuration, (a)CV cures of composite at different scan rates, (b) Ragone plots of our electrode at different scan rates, (c) GCD curves at various current density, (d) Specific volume capacitance at various current density.

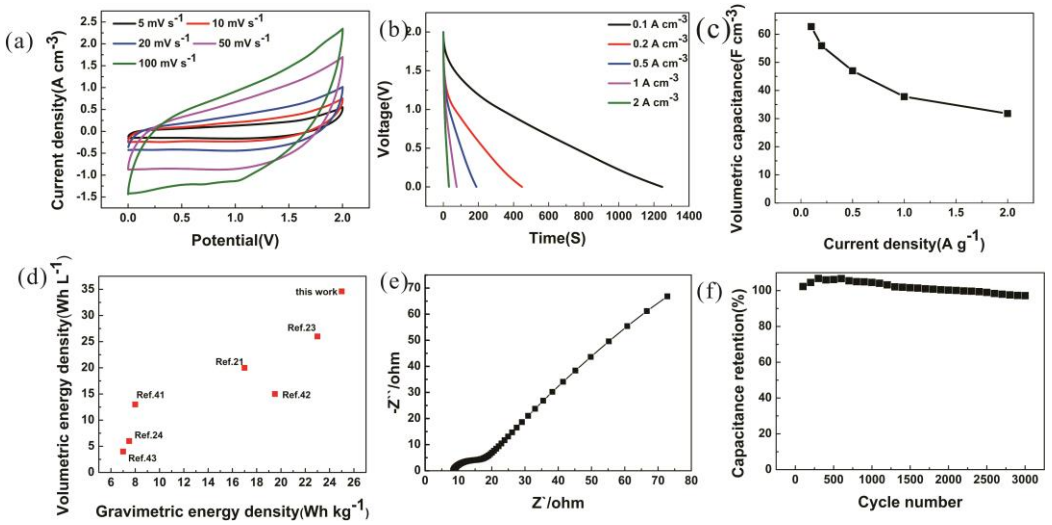

Fig. 6 (a) CV curves of the ASC based on MnO2@rGO and MoO3@rGO composite electrodes, (b) Discharge curves of the ASC at different current densities, (c) Volumetric capacitances of the ASC at different current density, (c) CV curves of the SASC at different scan rates, (d) Comparison of the volumetric and gravimetric capacitances of ASC with other carbon electrodes in aqueous electrolytes, (e) Nyquist plots of the ASC, (f) Cycle performance of the optimized ASC within a voltage window of 2.0 V at a scan rate of 50 mV s^{-1}.

with an AC perturbation of 10 mV (Fig. 6e). It exhibits a negligible 45º Warburg region, indicating fast ion transport at the interface of active materials-electrolyte. In the low frequency portion of the spectrum, the impedance spectra tend towards almost a vertical line where the imaginary part of impedance increases rapidly, showing the perfect capacitive behaviour of the ion diffusion in the electrode structure.[36] Long cycle life is an important requirement for supercapacitor. Fig. 6f shows the

cycle life test during 3000 cycles for ASC which was carried out by repeating the CV test between 0 and 2.0 V at a scan rate of 50 mV/s. The capacitance retention is 94.2% when the ASC cell stands 3000 cycles, which is much better than other pseudocapacitors.[37-39] It is worth noting that the specific capacitance sharply increases at the initial 400 cycles, which is probably related to an improvement in the surface wetting of the electrode by electrolyte and activation of the active materials.[40] This can be rationalized by hydrophobic nature of graphene.

Conclusions

We successfully develop an ASC using freestanding MnO_2@rGO and MoO_3@rGO film as positive and negative electrode, respectively. We demonstrate that coupling the MnO_2@rGO and MoO_3@rGO composites can produce ASCs with high energy and high output voltage in aqueous electrolyte. This hybridized nanostructure ASC presented here aims at freestanding, flexible and high energy density for applications which also maintains low cost and using environmental friendly materials practical applications. The simple fabricating process and the cell configuration of the ASC provide a promising research direction for low cost, environmental friendly, freestanding, flexible, high energy density, and high output voltage supercapacitors.

Acknowledgements

This work was supported by the National Basic Research Program (NO. 2011CB933300) of China, the National Natural Science Foundation of China(NO. 11204093 and 11374110), and the Fundamental Research Funds for the Central Universities (HUST: NO. 2014TS124).

Notes and references

1. F. Schedin, A. K. Geim, S. V. Morozov, E. W.Hill, P. Blake, M. I. Katsnelson and K. S. Novoselov, *Nature materials*, 2007, 6, 652-655.
2. I. Y. Kim, S. Park, H. Kim, S. Park, R. S. Ruoff and S.-J. Hwang, *Advanced Functional Materials*, 2014,24, 2288-2294.
3. D. Cohen-Tanugi and J. C. Grossman, *Nano letters*, 2012, 12, 3602-3608.
4. Z. Fan, J. Yan, T. Wei, L. Zhi, G. Ning, T. Li and F. Wei, *Advanced Functional Materials*, 2011, 21,2366-2375.
5. A. Balducci, R. Dugas, P. L. Taberna, P. Simon, D. Plée, M. Mastragostino and S. Passerini, *Journal of Power Sources*, 2007, 165, 922-927.
6. C. Liu, Z. Yu, D. Neff, A. Zhamu and B. Z. Jang, *Nano letters*, 2010, 10, 4863-4868.
7. L. Wei, M. Sevilla, A. B. Fuertes, R. Mokaya and G. Yushin, *Advanced Functional Materials*, 2012, 22,827-834.
8. P. J. Hall, M. Mirzaeian, S. I. Fletcher, F. B. Sillars, A. J. R. Rennie, G. O. Shitta-Bey, G. Wilson, A.Cruden and R. Carter, *Energy & Environmental Science*, 2010, 3, 1238.
9. N. Liu, W. Ma, J. Tao, X. Zhang, J. Su, L. Li, C. Yang, Y. Gao, D. Golberg and Y. Bando, *Advanced materials*, 2013, 25, 4925-4931.
10. J. Liu, L. Zhang, H. B. Wu, J. Lin, Z. Shen and X.W. Lou, *Energy Environ. Sci.*, 2014, 7, 3709-3719.
11. J. Tao, N. Liu, J. Rao, L. Ding, M. R. Al Bahrani,L. Li, J. Su and Y. Gao, *Nanoscale*, 2014, 6,15073-15079.
12. W. R. Zhong-Shuai Wu, Da-Wei Wang, Feng Li, Bilu Liu, and Hui-Ming Cheng, *ACS Nano*, 2010, 4,5835–5842.
13. M. T. Greiner, M. G. Helander, W. M. Tang, Z. B. Wang,J. Qiu and Z. H. Lu, *Nature materials*, 2012,11, 76-81.
14. M. L. P. Z. Viskadourakis, O. Conde, M. Zervos, and J. Giapintzakis, 2012.
15. C. A. Pan and T. P. Ma, *Applied Physics Letters*, 1980, 37, 714.
16. P. S. a. Y. Gogotsi, *Nature*, 2008, 7, 845.
17. F. Z. Dongqing Wu, Haiwei Liangab and Xinliang Feng, *Chemical Society reviews*, 2012, DOI:10.1039/c2cs35179j, 6160–6177.
18. M. Li, Z. Tang, M. Leng and J. Xue, *Advanced Functional Materials*, 2014, DOI:

10.1002/adfm.201402442, n/a-n/a.
19. C. Li and G. Shi, *Advanced materials*, 2014, DOI: 10.1002/adma.201306104.
20. J. Hu, Z. Kang, F. Li and X. Huang, *Carbon*, 2014, 67, 221-229.
21. J. R. M. a. P. Simon, *science*, 2008, 321, 651-652.
22. W. Wei, S. Yang, H. Zhou, I. Lieberwirth, X. Feng and K. Mullen, *Advanced materials*, 2013, 25,2909-2914.
23. L. Jiang, L. Sheng, C. Long and Z. Fan, *Nano Energy*, 2015, 11, 471-480.
24. E. Raymundo-Piñero, F. Leroux and F. Béguin, *Advanced materials*, 2006, 18, 1877-1882.
25. F. Yao, F. Gunes, H. Q. Ta, S. M. Lee, S. J. Chae,K. Y. Sheem, C. S. Cojocaru, S. S. Xie and Y. H. Lee,*Journal of the American Chemical Society*, 2012, 134, 8646-8654.
26. X. Yang, J. Zhu, L. Qiu and D. Li, *Advanced materials*, 2011, 23, 2833-2838.
27. X. Yang, L. Qiu, C. Cheng, Y. Wu, Z. F. Ma and D. Li, *Angewandte Chemie*, 2011, 50, 7325-7328.
28. Y. G. P. Simon, *Science*, 2011, 917–918.
29. Q. Qu, S. Yang and X. Feng, *Advanced materials*, 2011, 23, 5574-5580.
30. T. Brezesinski, J. Wang, S. H. Tolbert and B. Dunn, *Nature materials*, 2010, 9, 146-151.
31. W.-C. Chang, X. Qi, J.-C. Kuo, S.-c. Lee, S.-K. Ng and D. Chen, *CrystEngComm*, 2011, 13, 5125.
32. W. Tang, L. Liu, S. Tian, L. Li, Y. Yue, Y. Wu and K. Zhu, *Chemical communications*, 2011, 47, 10058-10060.
33. L. L. Z. Junyi Ji, Hengxing Ji, Yang Li,‡ Xin Zhao, Xin Bai, Xiaobin Fan, Fengbao Zhang, and Rodney S.Ruoff, *ACS Nano*, 2013, 7, 6237–6243.
34. Y. Tao, X. Xie, W. Lv, D. M. Tang, D. Kong, Z. Huang, H. Nishihara, T. Ishii, B. Li, D. Golberg, F. Kang, T.Kyotani and Q. H. Yang, *Sci Rep*, 2013, 3, 2975.
35. E. Raymundo-Piñero, M. Cadek and F. Béguin,*Advanced Functional Materials*, 2009, 19,1032-1039.
36. W. Chen, R. B. Rakhi, L. Hu, X. Xie, Y. Cui and H. N. Alshareef, *Nano letters*, 2011, 11, 5165-5172.
37. Q. W. Jing Xu, Xiaowei Wang, Qingyi Xiang, Bo Liang, Di Chen and Guozhen Shen, *ACS Nano*, 2013,7, 5453–5462.
38. W. C. Liangbing Hu, Xing Xie, Nian Liu, Yuan Yang, Hui Wu, Yan Yao, Mauro Pasta,Husam N. Alshareef,‡ and Yi Cui, *ACS Nano*, 2011, 5, 8904–8913.
39. J. K. S. W. Lee, S. Chen, P. T. Hammond and Y. Shao.Horn, *ACS Nano*, 2010, 4, 3889–3896.
40. F. Ataherian and N.-L. Wu, *Journal of The Electrochemical Society*, 2011, 158, A422.
41. G. Cheng, J. Xu, C.Dong, W. Yang, T. Kou and Z. Zhang, *J.Mater. Chem. A*, 2014, 2, 17307-17313
42. C. Dong, Y. Wang, J. Xu, G. Cheng, W. Yang, T. Kou, Z. Zhang and Y. Ding, *J.Mater.Chem. A*, 2014, 2, 18229-18235
43. C. Dong, Q. Bai, G.Cheng, B. Zhao, H. Wang, Y.Gao and Z. Zhang,*RSC Adv.*, 2015, 5,6207-6214